Conjugated Polyelectrolyte Thin Films for Pseudocapacitive Applications

Yip, Benjamin Rui Peng; Javier Vázquez, Ricardo; Jiang, Yan; McCuskey, Samantha R.; Quek, Glenn; Ohayon, David; Wang, Xuehang; Bazan, Guillermo C.

DOI
10.1002/adma.202308631

Publication date
2023

Document Version
Final published version

Published in
Advanced Materials

ADVANCED MATERIALS
www.advmat.de

Conjugated Polyelectrolyte Thin Films for Pseudocapacitive Applications

Benjamin Rui Peng Yip, Ricardo Javier Vázquez, Yan Jiang, Samantha R. McCuskey, Glenn Quek, David Ohayon, Xuehang Wang, and Guillermo C. Bazan**

A subclass of organic semiconductors known as conjugated polyelectrolytes (CPEs) is characterized by a conjugated backbone with ionic pendant groups. The water solubility of CPEs typically hinders applications of thin films in aqueous media. Herein, it is reported that films of an anionic CPE, namely CPE-K, drop cast from water produces single-component solid-state pseudocapacitive electrodes that are insoluble in aqueous electrolyte. That X-ray diffraction experiments reveal a more structurally ordered film, relative to the as-obtained powder from chemical synthesis, and dynamic light scattering measurements show an increase in aggregate particle size with increasing [KCl] indicate that CPE-K films are insoluble because of tight interchain contacts and electrostatic screening by the electrolyte. CPE-K film electrodes can maintain 85% of their original capacitance (84 F g^{-1}) at 500 A g^{-1} and exhibit excellent cycling stability, where a capacitance retention of 93% after 100 000 cycles at a current density of 35 A g^{-1}. These findings demonstrate that it is possible to use initially water soluble ionic-organic materials in aqueous electrolytes, by increasing the electrolyte concentration. This strategy can be applied to the application of conjugated polyelectrolytes in batteries, organic electrochemical transistors, and electrochemical sensors, where fast electron and ion transport are required.

1. Introduction

Current electrochemical energy storage technologies cannot match the energy and power output of internal combustion engines efficiently and reliably.[1] Batteries are the leading platform for electrochemical energy storage as they can provide high energy densities (≈100 Wh kg^{-1}) by storing charges through faradaic processes. However, batteries are limited by diffusion-controlled kinetics, resulting in low power densities (≈10^2 W kg^{-1}).[2] Supercapacitors store charges through surface-controlled processes, such as electrostatic adsorption, surface redox reaction, and pseudocapacitive intercalation, which allow supercapacitors to exhibit high power densities (≈10^4 W kg^{-1}) and long cycling life.[3–6] However, mainstream electrification depends on developing materials that can deliver high energy densities without sacrificing power densities and cycling stability.[3,4,7,8]

Pseudocapacitive materials hold the promise to deliver intermediate power and energy densities simultaneously, occupying a niche position between batteries and electric double layer capacitors.[5,6] Pseudocapacitive properties arise from rapid near-surface redox reactions and counter ion intercalation/adsorption into or onto the material to stabilize the electronic charge, allowing it to have faster kinetics than battery materials.[9] Representative pseudocapacitive materials include transition metal oxides,[10,11] sulfides and nitrides,[12,13] covalent organic frameworks,[14] MXenes,[15] and related composites.[16,17] Organic semiconducting materials have also attracted interest due to alternative processing options and the ability to form flexible electrodes. One class of such materials are conjugated

B. R. P. Yip, R. Javier Vázquez, Y. Jiang, S. R. McCuskey, G. Quek, D. Ohayon, G. C. Bazan
Departments of Chemistry and Chemical and Biomolecular Engineering
National University of Singapore
Singapore 119077, Singapore
E-mail: bazan@chem.ucsb.edu
B. R. P. Yip, R. Javier Vázquez, Y. Jiang, S. R. McCuskey, G. Quek, D. Ohayon, G. C. Bazan
Institute for Functional Intelligent Materials
National University of Singapore
Singapore 117544, Singapore
S. R. McCuskey, G. C. Bazan
Singapore Centre for Environmental Life Sciences Engineering
Nanyang Technological University
Singapore 639798, Singapore
X. Wang
Department of Radiation Science and Technology
Delft University of Technology
Delft 2629 JB, The Netherlands
E-mail: x.wang-22@tudelft.nl
G. C. Bazan
Department of Chemistry and Biochemistry
University of California
Santa Barbara, CA USA
The ORCID identification number(s) for the author(s) of this article can be found under https://doi.org/10.1002/adma.202308631

DOI: 10.1002/adma.202308631

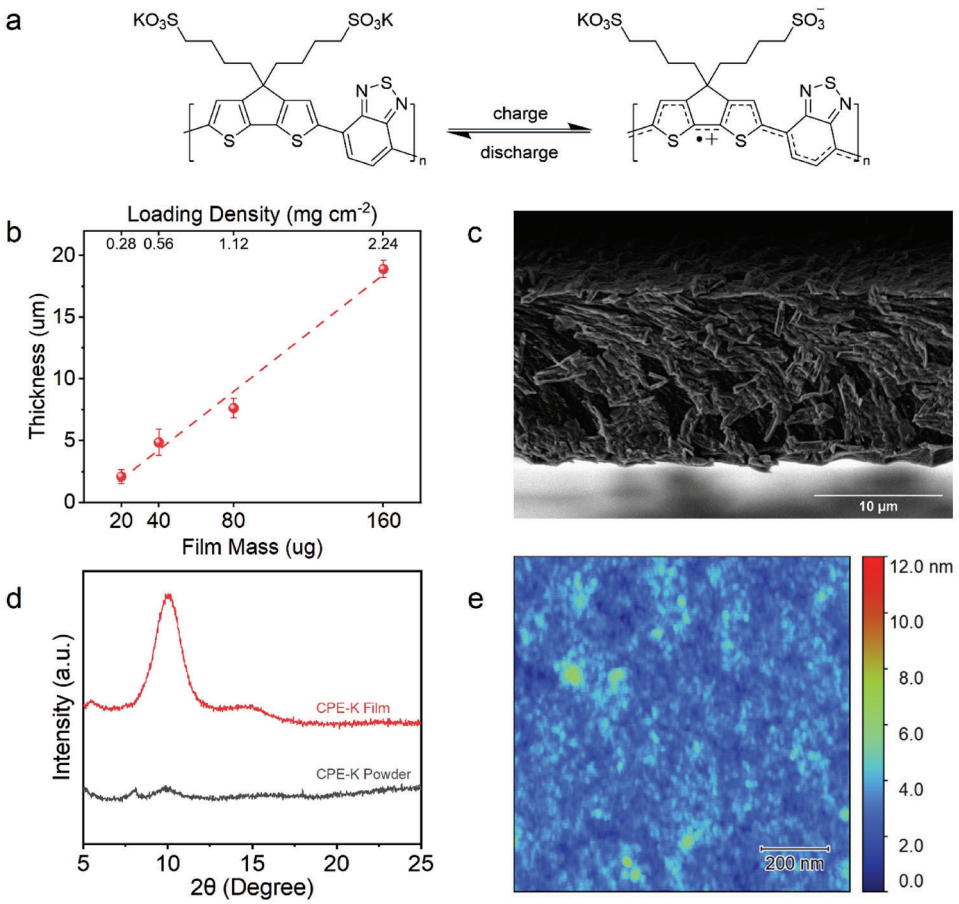

Figure 1. a) Mechanism of reversible pseudocapacitive charge storage in CPE-K. b) Thickness measurements of CPE-K films as a function of mass loading measured by profilometry. c) Cross-sectional SEM image of pristine CPE-K film deposited on ITO glass (2.24 mg cm^{-2}). d) X-Ray diffraction pattern of CPE-K film (2.24 mg cm^{-2}) compared to its prefabricated powder form. e) Atomic Force Microscope image of pristine CPE-K film surface deposited on glassy carbon electrode (0.28 mg cm^{-2}).

polymers (CPs), which exhibit pseudocapacitance by reversible doping/de-doping processes accompanied by counter ion intercalation/adsorption into the bulk material.[18,19] However, most CPs are undoped in their neutral state, leading to low electronic conductivities which give rise to limited rates.[20] In addition, repeated ion intercalation/adsorption between charge cycles lead to challenges in cycling performance when compared to inorganic counterparts.[20] One example is PANi with a specific capacitance of 480 F g^{-1} at a specific current of 1 A g^{-1}, which maintains ≈70% of its specific capacitance at 10 A g^{-1}.[21] Furthermore, PANi has been shown to have a cycling performance of ≈50% retention after 1000 charge/discharge cycles. To address challenges of this type, strategies have emerged to improve the rate performance and cycling stability of CPs by incorporating carbon based composites[22–24] and/or morphology control.[25–27]

Conjugated polyelectrolytes (CPEs) are conjugated polymers with ionizable pendant side chains that give rise to different physico–chemical properties, relative to their neutral counterparts.[28] They form part of a set of materials known as organic mixed ionic–electronic conductors, which exhibit the ability to simultaneously conduct ions and electronic charges.[29,30] CPEs thus possess properties that may grant them unique advantages over conventional conjugated polymers, including water processability, self-doping properties, and enhanced ionic conductivity. It is the latter two properties that may allow CPEs to stand out from conventional conjugated polymers in terms of electrochemical energy storage applications. Previous efforts have shown that the anionic CPE known as CPE-K, see **Figure 1**a, in its hydrogel form exhibits a specific capacitance of 85 F g^{-1} and retains 76% of the initial capacitance after 100 000 cycles at 2.5 A g^{-1}.[31–33] However, the electrochemical properties have yet to be investigated in the solid-state form, since spun coated films were initially anticipated to redissolve in pure water.

We report here that slow-evaporation from water solution promotes the formation of crystalline domains in the CPE-K thin films. Moreover, CPE-K films are stable in KCl electrolyte at concentrations higher than 0.1 M. Thin-film electrodes based on CPE-K possess a specific capacitance of 82 ± 2 F g^{-1} with capacitance retention of 93% after 100 000 cycles at a rate of 35 A g^{-1}. The use of aqueous electrolytes, along with water processability, could allow the development of CPE based pseudocapacitive materials with differentiated properties within the context of sustainability.

2. Results and Discussion

2.1. Fabrication and Characterization of CPE-K Films

CPE-K was synthesized as previously reported.[31] Briefly, molar equivalent amounts of potassium 4,4′-(2,6-dibromo-4H-cyclopenta[2,1-b:3,4-b′]dithiophene-4,4-diyl)*bis*(butane-1-sulfonate) and 2,1,3-benzothiadiazole4,7-*bis*(boronic acid pinacol ester) were polymerized under Suzuki cross-coupling conditions (see Supporting Information). The resulting crude CPE-K was purified by dialysis (MWCO = 3500 kDa) and was subsequently lyophilized to obtain a metallic-looking dark blue powder that is soluble in H_2O and insoluble in common polar organic solvents. To fabricate electroactive films on a glassy carbon electrode (GCE; ø = 3.0 mm), CPE-K was dissolved in Milli-Q water to obtain solutions of concentrations ranging from 2.0–16.0 mg mL^{-1}.

Thereafter, the CPE-K solution was drop cast on polished GCE surfaces and was allowed to slow-dry overnight under ambient conditions. Dark blue films were thus obtained, which were used in subsequent studies without further treatment. By this method we obtained CPE-K films with mass loadings of 20, 40, 80, and 160 µg, as obtained by drop casting 10 µL of polymer solution at concentrations of 2.0, 4.0, 8.0, and 16.0 mg mL^{-1}, respectively. The CPE-K films will be referred to CPE-K/20, CPE-K/40, CPE-K/80, and CPE-K/160, respectively, from now on, named after the mass loading in micrograms. These films have loading densities ranging from 0.28 to 2.24 mg cm^{-2} (Figure 1b), calculated based on the area of the GCE surface (≈0.0707 cm^{-2}). This corresponds to the same order of magnitude as required for practical applications (>1.0 mg cm^{-2}).[34] Using a stylus profilometer directly on the GCE revealed that the thickness of the CPE-K films range from ≈2.1 ± 0.6 to 19.0 ± 0.7 µm (Figure 1b), which are within the range of typical coin cell electrodes (<26 µm).[35] A linear relationship between film thickness and mass loading density can be seen in Figure 1b, from which the slope can be used to obtain a gravimetric density of ≈1.23 g cm^{-3}, consistent with what has been observed with other conjugated polymer films.[36,37] The cross-section of the films was also imaged by SEM and the thicknesses obtained were close to profilometry measurements (Figure 1c).

X-ray diffraction measurements were performed with CPE-K in its pre-deposited powder form and with CPE-K films (see Supporting Information). The CPE-K film exhibited a strong peak at 10.1° indicative of ordered domains that is not observed in the powder form (Figure 1d). Our current thinking is that the slow-drying process enables dynamic processes in solution that favor organization of crystalline domains. Conversely, the purification process to obtain CPE-K powder includes precipitation, dialysis, and lyophilization, which presumably lock the polymer in a more soluble disordered state. The diffraction peak at $2\theta = 10.1°$ corresponds to a Bragg spacing of $d = 8.8$ Å. This agrees with previously reported GIWAXS measurements on spin coated CPE-K films, which also exhibited similar scattering features ($q_z = 0.75$ $Å^{-1}$, $d = 8.3$ Å).[38] Notably, this peak is not due to lattices typically observed in neutral conjugated polymers, for example corresponding to lamellar spacing or π-π stacking. Instead, it is reasonable to assign the feature to an ionic lattice stemming from the presence of ionic functional groups. This assignment is also supported by It is also relevant to point out a previous report that studied in detail the structure of CPE-K in its hydrogel state and found that unstructured aromatic interactions and electrostatic interactions comprise the driving force for self-assembly.[39] Therefore, it is reasonable that the films formed via drop casting evolve their final structure from this morphology, since drying from solution under ambient conditions will cause the solution to self-assemble into its hydrogel form on the way to forming the film.

Thermogravimetric analysis shows that CPE-K film has more water content than CPE-K powder based on the ≈5.5% and 11.5% weight loss at 150 °C, respectively (Figure S5, Supporting Information). This suggests that hydration of ions in the film state is an important component of the final structure, and that water may aid in achieving the final organization. As a result, the first heating traces in the differential scanning calorimetry measurements are dominated by the enthalpy of water desorption and fail to reveal any melting transitions in either the thin film or powder forms of CPE-K (Figure S5, Supporting Information). Indeed, this challenge in obtaining insights into the thermophysical properties of conjugated polyelectrolytes has been reported previously.[40]

We subsequently investigated the effect of salt concentration on the stability of CPE-K films. We found that CPE-K films were susceptible to dissolution when immersed into electrolytes of low ionic strength (<0.1 M KCl). Conversely, CPE-K films were found to be stable at higher salt concentrations (≥0.1 M KCl). Related to these observations is the increased aggregation of CPE-K in aqueous solution with increasing salt concentrations as determined DLS (see Supporting Information). These studies showed that the aggregate particle size increases from 10^1 to 10^3 nm as [KCl] increased from 1 mM to 1.0 M (Figure S10, Supporting Information). This phenomenon can be explained by electrostatic screening which occurs in the presence of excess K^+ ions. This decreases the extent of repulsion between the sulfonate pendant groups of the conjugated polyelectrolyte and, in turn, suppresses the solubility of CPE-K films.[41,42] Despite the evidence of crystalline domains (Figure 1d), CPE-K films possess a relatively flat surface with an RMS of 0.71 nm, as revealed by atomic force microscopy (Figure 1e). Overall, that CPE-K films are stable in aqueous electrolytes is attributed to a more ordered morphology upon slow drying and the electrostatic screening between the sulfonate pendant groups by the excess K^+ ions once a critical concentration is achieved.

2.2. Electrochemical Characterization

The electrochemical performance of the CPE-K films was evaluated by galvanostatic charge/discharge (GCD) measurements. Electrochemical measurements were performed using a 3-electrode cell setup in 2.0 M KCl using an Ag/AgCl reference electrode and carbon felt as the counter electrode (see Supporting Information). A potential of 0.6 V versus Ag/AgCl was applied for 300 s before GCD measurements with the purpose of saturating the CPE-K film with ions. GCD measurements from 0.0 to 0.6 V versus Ag/AgCl exhibited a trace, which was non-linear below a potential of 0.2 V versus Ag/AgCl (Figure S11, Supporting Information). Therefore, the potential window selected for

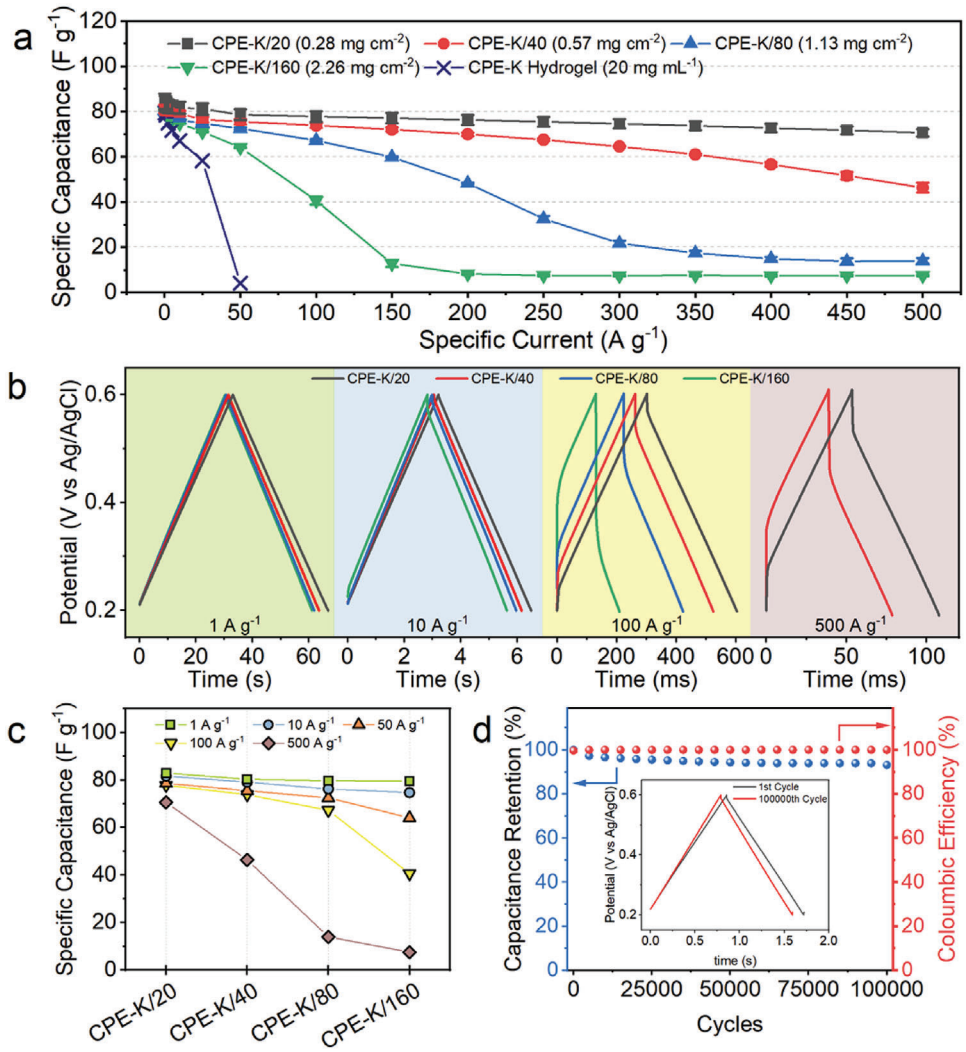

Figure 2. Electrochemical measurements were performed using a 3-electrode cell setup with an Ag/AgCl reference electrode and carbon felt as a counter electrode in 2.0 M KCl. a) The specific capacitance of CPE-K films as a function of specific current determined by GCD. b) Representative GCD trace for CPE-K films at 1, 10, 100, and 500 A g^{-1}. c) The specific capacitance at various current densities as a function film thickness. d) The cycling stability test of CPE-K/20 film at a current density of 35 A g^{-1}.

GCD measurements was chosen from 0.2 to 0.6 V, since a linear charge/discharge response was observed in this range. The specific capacitance, C_s, can be calculated using Equation (1).

$$C_S = \frac{I\Delta t}{m\Delta V} \tag{1}$$

where I is the constant discharging current, Δt is the discharge time, m is the mass of CPE-K, and ΔV is the magnitude of the change in potential during discharging (excluding any IR drop). Reference to **Figure 2**a reveals that the C_s values for the films do not differ within statistical certainty in this specific current range (0.25–10 A g^{-1}) and converge to ≈82 ± 2 F g^{-1}.[31,33] All CPE-K films exhibit GCD traces with a triangular-shaped profile with negligible IR drop (Figure 2b) below 10 A g^{-1}.

Capacitance decay as a function of film thickness was observed at a given specific current (Figure 2a,c). For example, CPE-K films show C_s values of 78, 74, 67, and 41 F g^{-1}, at 100 A g^{-1} which, relative C_s at 10 A g^{-1}, correspond to capacitance losses of 8%, 9%, 16%, and 51% in order of increasing thickness. The loss of capacitance was mainly due to IR drop as seen from deviations from an ideal triangular-shaped profile as a function of thickness and charging rate (Figure 2b). As an illustration, we note that the magnitude of the IR drops at 100 A g^{-1} are 230 and 120 mV for CPE-K/160 and CPE-K/80, respectively and are less pronounced for CPE-K/40 and CPE-K/20 films, at 60 and 30 mV, respectively. Of relevance is that CPE-K/40 and CPE-K/20 films can still exhibit a capacitive performance of 46 and 71 F g^{-1} at 500 A g^{-1}, albeit with IR drops of 140 and 65 mV, respectively. Hence, a capacitance retention of 57% and 84% has been obtained for CPE-K/40 and CPE-K/20 films up to 500 A g^{-1}. Of particular significance is that all films showed less than 20% capacitance decay at 50 A g^{-1}, which highlights the excellent rate performance of CPE-K films (Figure 2c). For clarity, Table S2 (Supporting Information)

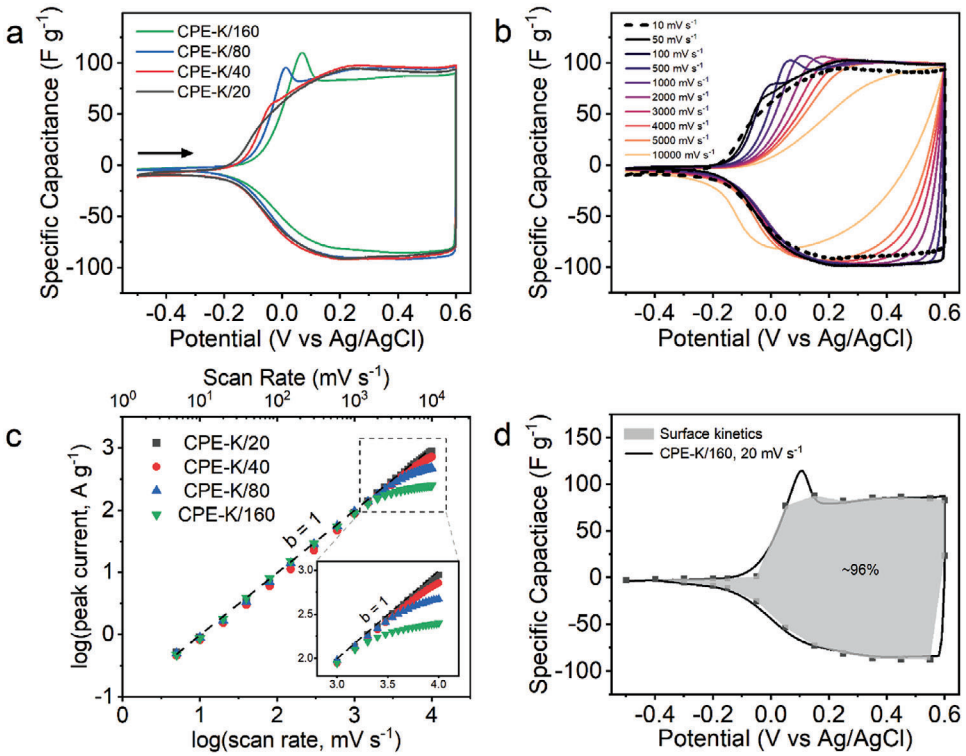

Figure 3. Electrochemical measurements were performed using a 3-electrode cell setup with an Ag/AgCl reference electrode and carbon felt as a counter electrode in 2.0 M KCl. a) Representative cyclic voltammograms of CPE-K films at 10 mV s^{-1}. b) Cyclic voltammogram of CPE-K/20 film from 10–10 000 mV s^{-1} (See Supporting Information for other film thickness). c) Log–log plots of peak current density versus the scan rate as a function of CPE-K film thickness. d) Proportion of surface-controlled capacitance of CPE-K/160 at 20 mV s^{-1}.

summarizes the rate performance and other relevant aspects of single component conjugated polymers in the context of energy storage.

Cycling stability was evaluated using prolonged GCD cycles. The specific current selected for evaluating the cycling stability was 35 A g^{-1} for CPE-K/20 as it shows the highest specific capacitance (80 F g^{-1}). These studies revealed that CPE-K/20 exhibits a C_s retention of 93% after 100 000 cycles (Figure 2d). In addition, coulombic efficiencies of more than 99% were observed over the course of the cycling stability test for CPE-K/20 (Figure 2d), which confirms minimal degradation under prolonged cycling.

Cyclic voltammetry (CV) was used to gain insight into the charge storage kinetics. Qualitative scans from −0.5 to 0.6 V versus Ag/AgCl were initially carried out on all film thickness at a scan rate of 10 mV s^{-1} (**Figure 3**a). These scans show a reversible, quasi-rectangular shape profile combined with a "tail" before the onset potential, in agreement with a pseudocapacitive charge storage mechanism.[31,33,43] Additional CVs with a similar potential window to GCD (0.0 to 0.6 V vs Ag/AgCl) were also carried out to further highlight the quasi-rectangular shape profile (Figure S11, Supporting Information). One feature that was observed with increasing thickness is an increase in the onset potential and appearance of a oxidation peak. This phenomenon is associated with hole transport/charge transfer resistance in mixed ionic and electronic conductors.[44] Note that the films show a gradual loss of quasi-rectangular shape at increasing scan rates (Figure 3b and Supporting Information).

The relationship between the response current and the scan rate obeys the power law in Equation (2):

$$i = av^b \tag{2}$$

where i is the peak current obtained from the cyclic voltammogram, a is an arbitrary constant and v is the scan rate, and b is a value between 0.5 and 1.0, which gives information on the charge storage kinetics. Generally, b-values close to 1.0 indicate surface-controlled kinetics, whereas a b-value close to 0.5 is attributed to the presence of diffusion-limited process.[34] At scan rates up to 1000 mV s^{-1}, a linear dependence of peak current on the scan rate ($b \approx 1$) is observed regardless of thickness, indicating surface-level charge storage mechanism (Figure 3c). At scan rates >1000 mV s^{-1}, CPE-K/40 and CPE-K/20 still exhibit a linear peak current versus scan rate relationship, up to 8000 and 10 000 mV s^{-1}, respectively. The dependence of peak current on the scan rate for thicker films, that is, CPE-K/80 and CPE-K/160, showed deviation from unity above 3000 and 1000 mV s^{-1}, respectively. This reflects a reduced conductivity or increased charge transfer resistance in the thicker films.[45]

The proportion of surface controlled versus diffusion-controlled current can be deconvoluted based on Equation (3).

$$i = k_1 v + k_2 v^{1/2} \tag{3}$$

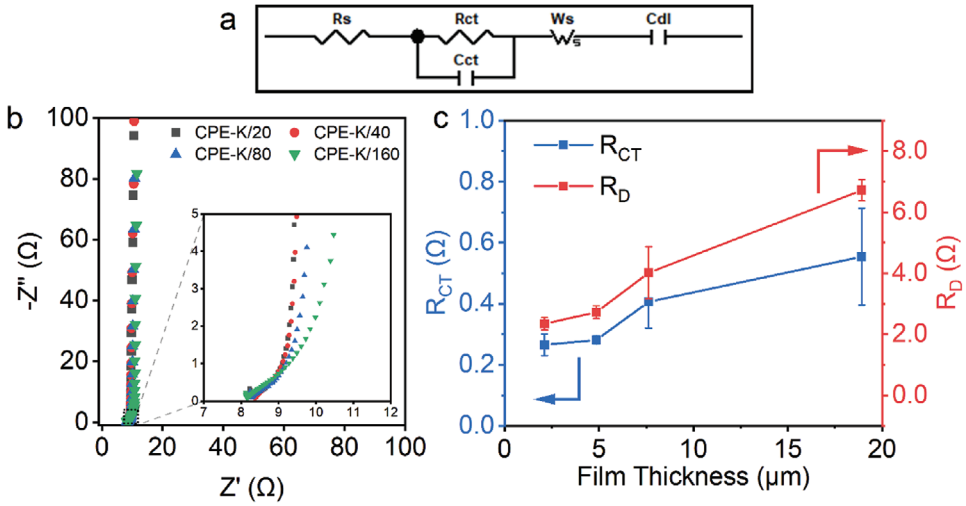

Figure 4. Results of electrochemical impedance data of CPE-K films of different thicknesses. a) The equivalent circuit used for modeling; b) Representative Nyquist plot with enlarged high-frequency region; c) Correlated increase of R_{CT} and R_D as a function of increasing thickness. Values were obtained from equivalent circuit fitting.

where i is the current density at a specific potential in CV, v is the scan rate, and k_1 and k_2 are constants that can be derived from the slope and the intercept from the linear plot of $i/v^{1/2}$ as a function of $v^{1/2}$. From the results of this analysis, the proportion of capacitance arising from surface-controlled redox reactions of ≈96% was obtained, even for CPE-K/160 (Figure 3d). These results on the whole indicate fast and reversible electronic and ionic transport within the films albeit with a non-negligible ohmic loss at higher scan rates and/or specific currents, which is more evident in the thicker films.

Electrochemical impedance spectroscopy (EIS) was used to gain further insight into the electronic and ionic resistances of the system. EIS was conducted at a potential of 0.3 V versus Ag/AgCl. No evident charge transfer semi-circle was observed in all film thicknesses, which suggests an interfacial charge transfer resistance of <1.0 Ω (Figure S7, Supporting Information).[34,44] On closer inspection, one observes a Warburg region which did not increase significantly despite a thickness increase of eight times. Therefore, we used a finite length diffusion or short Warburg (W_s) to model the Nyquist plot of the thin films, which is defined by Equation (4).[46]

$$W_s = R_D \frac{\coth\sqrt{j\omega\tau_D}}{\sqrt{j\omega\tau_D}} \tag{4}$$

where j is $(-1)^{1/2}$, ω is the angular frequency, τ_D is the diffusion time constant, and R_D is the diffusional resistance. In addition, there is an associated diffusional pseudocapacitance which can be described by Equation (5).[46]

$$C_D = \frac{\tau_D}{R_D} \tag{5}$$

where C_D is the diffusional pseudocapacitance. Components used for the EIS circuit include R_s which describes equivalent series resistance (ESR), a charge transfer element made by R_{CT} and C_{CT} circuit in parallel, and C_{DL} which describes the double-layer capacitance upon doping of CPE-K (**Figure 4**a). This circuit has been used to model similar systems with varying thicknesses successfully.[46,47] In fact, when this model was applied to our system, excellent fits were obtained with χ^2 (goodness of fit) values of <0.1.

Table 1 summarizes the results from the equivalent circuit fitting. Here, R_s (ESR) is found to be independent of the film thickness. This observation agrees with previously reported work, where R_s is weakly thickness dependent but instead, inversely proportional to the electroactive surface area.[47,48] In contrast, all other parameters exhibit strong dependence on the film thickness. The charge transfer resistance (R_{CT}) is small (<1.0 Ω) even for CPE-K/160. Similarly, the diffusional resistance (R_D) scales with an increase in film thickness due to the increased distance that the ions have to travel. It is worth noting that R_{CT} and R_D scale almost proportionally with each other (Figure 4c). We believe this to be due to the presence of strong ionic–electronic coupling within the CPE-K films which is known to be present in mixed ionic–electronic conductors.[29]

The diffusion time constant τ_D is related to the diffusion coefficient (D) and diffusion length (L), and is related by Equation (6)

$$\tau_D = \frac{L^2}{D} \tag{6}$$

Initially, we expected that the diffusion coefficient (D) would be consistent throughout all thicknesses. However, this is not observed from circuit fitting results and instead an increase in the apparent diffusion coefficient (D) along with diffusion length (L) was observed. One possible explanation could be that the diffusion length (L) is shorter than the thickness of the film, indicating that the film is easily accessible to ions. Another explanation could be that a larger volume of film could swell to a greater extent and allow faster ion diffusion within the film.[49] It is worth noting, that if we assume the diffusion length (L) to be the thickness

Table 1. Results from equivalent circuit fitting of electrochemical impedance measurements in 2.0 M KCl electrolyte.

	R_s [Ω]	R_{CT} [Ω]	R_D [Ω]	τ_D[s]	C_{DL} [mF]	$L^{a)}$ [μm]	$D^{b)}$ [$\times 10^{-6}$ cm^2 s^{-1}]
CPE-K/20	7.82	0.265	2.34	0.013	2.32	2.1	3.95
CPE-K/40	7.82	0.281	2.72	0.030	4.19	4.9	6.09
CPE-K/80	7.90	0.406	4.01	0.079	8.76	7.6	7.38
CPE-K/160	7.75	0.554	6.72	0.248	18.27	18.9	14.46

[a)] Determined by profilometry and cross-sectional SEM; [b)] Calculated based on film thickness L and Equation (6).

of the film, the calculated diffusion coefficients within the film approach the diffusivity of Cl^- in water of similar concentration (2.0×10^{-5} cm^2 s^{-1}, Table 1).[50,51] In fact, a similar impedance studies of PEDOT:PSS resulted in diffusion coefficients of comparable magnitude.[46,47] This feature may be the reason for the enhanced rate performance of CPE-K films when compared to its hydrogel form.

3. Conclusion

In summary, it is possible to use CPE-K to fabricate thin-film pseudocapacitive electrodes with high-performance operability in aqueous electrolytes. That the films can be prepared from water, yet are stable in aqueous electrolyte media, is attributed to an increased interchain order, due to slow evaporation, and a decrease of electrostatic repulsion between chains due to the presence of electrolyte ions. The latter point is supported by DLS studies that demonstrate how increasing the salt concentration in aqueous solutions of CPE-K leads to more pronounced aggregation. CPE-K films have a specific capacitance that converges to 82 F g^{-1} regardless of loading density. A 2 μm thick CPE-K film can be charged at rates as high as 500 A g^{-1}, while maintaining 85% of its original capacitance (84 F g^{-1}). At a typical mass loading (1.12 mg cm^{-2}, thickness ≈ 8 μm), it was possible to charge the CPE-K electrode at 100 A g^{-1} while maintaining 67 F g^{-1}. Such performance enables cycling of CPE-K films at higher current densities than those used for other conjugated polymers. Cycling stability measurements showed that CPE-K films retain 93% of its original capacitance after 100 000 cycles when cycled at 35 A g^{-1}. Cyclic voltammetry measurements revealed that surface-controlled pseudocapacitive behavior dominates the CPE-K electrodes, since $b \approx 1$ was obtained in scan rates up to 1 V s^{-1} for all the mass loadings in this study. CV and EIS characterization suggest facile ionic diffusion within the CPE-K films. We attribute this to the presence of an ionic lattice in the ordered structure of the CPE-K films, which can enhance the transport of ions. These findings provide a new perspective for the applications of organic mixed ionic–electronic conductors typically not used as solid-state materials in the presence of aqueous electrolytes. The strategy of decreasing water solubility by controlling counterion condensation and/or electrostatic screening opens opportunities in applications such as batteries, organic electrochemical transistors, or electrochemical sensors, where fast electron transfer and ion transport are desired.

Supporting Information

Supporting Information is available from the Wiley Online Library or from the author.

Acknowledgements

This research was supported by the Ministry of Education, Singapore, under its Research Centre of Excellence award to the Institute for Functional Intelligent Materials (I-FIM, project No. EDUNC-33-18-279-V12) and by the National University of Singapore start-up grant A-0004525-00-00.

Conflict of Interest

The authors declare no conflict of interest.

Data Availability Statement

The data that support the findings of this study are available in the supplementary material of this article.

Keywords

conjugated polyelectrolytes, cycling stability, high-rate capability, pseudocapacitors

Received: August 24, 2023
Revised: October 28, 2023
Published online:

[1] Q. Zhen, S. Bashir, J. L. Liu, *Nanostructured Materials for Next-Generation Energy Storage and Conversion: Advanced Battery and Supercapacitors*, 1st ed. Springer, Berlin **2019**.
[2] P. Simon, Y. Gogotsi, *Nat. Mater.* **2008**, *7*, 845.
[3] R. Kötz, M. Carlen, *Electrochim. Acta* **2000**, *45*, 2483.
[4] W. G. Pell, B. E. Conway, *J. Power Sources* **2004**, *136*, 334.
[5] Z. Yu, L. Tetard, L. Zhai, J. Thomas, *Energy Environ. Sci.* **2015**, *8*, 702.
[6] Y. Jiang, J. Liu, *Energy Environ. Mater.* **2019**, *2*, 30.
[7] J. F. Mike, J. L. Lutkenhaus, *J. Polym. Sci., Part B: Polym. Phys.* **2013**, *51*, 468.
[8] Z. Zhai, L. Zhang, T. Du, B. Ren, Y. Xu, S. Wang, J. Miao, Z. Liu, *Mater. Des.* **2022**, *221*, 111017.
[9] S. Fleischmann, J. B. Mitchell, R. Wang, C. Zhan, D.-E. Jiang, V. Presser, V. Augustyn, *Chem. Rev.* **2020**, *120*, 6738.
[10] C.-H. Lai, D. Ashby, M. Moz, Y. Gogotsi, L. Pilon, B. Dunn, *Langmuir* **2017**, *33*, 9407.
[11] Y. Zhao, M. P. Li, S. Liu, M. F. Islam, *ACS Appl. Mater. Interfaces* **2017**, *9*, 23810.
[12] D. Choi, G. E. Blomgren, P. N. Kumta, *Adv. Mater.* **2006**, *18*, 1178.
[13] J. B. Cook, H.-S. Kim, T. C. Lin, C.-H. Lai, B. Dunn, S. H. Tolbert, *Adv. Energy Mater.* **2017**, *7*, 1601283.
[14] J. C. Russell, V. A. Posey, J. Gray, R. May, D. A. Reed, H. Zhang, L. E. Marbella, M. L. Steigerwald, Y. Yang, X. Roy, C. Nuckolls, S. R. Peurifoy, *Nat. Mater.* **2021**, *20*, 1136.

[15] E. Kayali, A. Vahidmohammadi, J. Orangi, M. Beidaghi, *ACS Appl. Mater. Interfaces* **2018**, *10*, 25949.
[16] Y. Zhou, K. Maleski, B. Anasori, J. O. Thostenson, Y. Pang, Y. Feng, K. Zeng, C. B. Parker, S. Zauscher, Y. Gogotsi, J. T. Glass, C. Cao, *ACS Nano* **2020**, *14*, 3576.
[17] S. Lee, X. Jin, I. Y. Kim, T.-H. Gu, J.-W. Choi, S. Nahm, S.-J. Hwang, *J. Phys. Chem. C* **2016**, *120*, 11786.
[18] G. Wang, L. Zhang, J. Zhang, *Chem. Soc. Rev.* **2012**, *41*, 797.
[19] Y. Zhao, B. Liu, L. Pan, G. Yu, *Energy Environ. Sci.* **2013**, *6*, 2856.
[20] Q. Zhang, A. Zhou, J. Wang, J. Wu, H. Bai, *Energy Environ. Sci.* **2017**, *10*, 2372.
[21] H. R. Ghenaatian, M. F. Mousavi, S. H. Kazemi, M. Shamsipur, *Synth. Met.* **2009**, *159*, 1717.
[22] C. Tran, R. Singhal, D. Lawrence, V. Kalra, *J. Power Sources* **2015**, *293*, 373.
[23] M. Hassan, K. R. Reddy, E. Haque, S. N. Faisal, S. Ghasemi, A. I. Minett, V. G. Gomes, *Compos. Sci. Technol.* **2014**, *98*, 1.
[24] C.-M. Chang, C.-J. Weng, C.-M. Chien, T.-L. Chuang, T.-Y. Lee, J.-M. Yeh, Y. Wei, *J. Mater. Chem. A* **2013**, *1*, 14719.
[25] J. Mu, G. Ma, H. Peng, J. Li, K. Sun, Z. Lei, *J. Power Sources* **2013**, *242*, 797.
[26] S. K. Simotwo, V. Kalra, *Curr. Opin. Chem. Eng.* **2016**, *13*, 150.
[27] X. Wang, J. Deng, X. Duan, D. Liu, J. Guo, P. Liu, *J. Mater. Chem. A* **2014**, *2*, 12323.
[28] G. Quek, B. Roehrich, Y. Su, L. Sepunaru, G. C. Bazan, *Adv. Mater.* **2022**, *34*, 2104206.
[29] B. D. Paulsen, K. Tybrandt, E. Stavrinidou, J. Rivnay, *Nat. Mater.* **2020**, *19*, 13.
[30] S. T. M. Tan, A. Gumyusenge, T. J. Quill, G. S. Lecroy, G. E. Bonacchini, I. Denti, A. Salleo, *Adv. Mater.* **2022**, *34*, 2110406.
[31] R. J. Vázquez, G. Quek, S. R. Mccuskey, L. Llanes, B. Kundukad, X. Wang, G. C. Bazan, *J. Mater. Chem. A* **2022**, *10*, 21642.
[32] G. Quek, Y. Su, R. K. Donato, R. J. Vázquez, V. S. Marangoni, P. R. Ng, M. C. F. Costa, B. Kundukad, K. S. Novoselov, A. H. C. Neto, G. C. Bazan, *Adv. Electron. Mater.* **2022**, *8*, 2100942.
[33] Y. Su, S. R. Mccuskey, D. Leifert, A. S. Moreland, L. Zhou, L. C. Llanes, R. J. Vazquez, L. Sepunaru, G. C. Bazan, *Adv. Funct. Mater.* **2021**, *31*, 2007351.
[34] T. S. Mathis, N. Kurra, X. Wang, D. Pinto, P. Simon, Y. Gogotsi, *Adv. Energy Mater.* **2019**, *9*, 1902007.
[35] L. Ke, W. Lv, F.-Y. Su, Y.-B. He, C.-H. You, B. Li, Z. Li, Q.-H. Yang, F. Kang, *Carbon* **2015**, *92*, 311.
[36] F. Machui, S. Rathgeber, N. Li, T. Ameri, C. J. Brabec, *J. Mater. Chem.* **2012**, *22*, 15570.
[37] S. Hiura, N. Okada, J. Wakui, H. Narita, S. Kanehashi, T. Shimomura, *Materials* **2017**, *10*, 468.
[38] C.-K. Mai, R. A. Schlitz, G. M. Su, D. Spitzer, X. Wang, S. L. Fronk, D. G. Cahill, M. L. Chabinyc, G. C. Bazan, *J. Am. Chem. Soc.* **2014**, *136*, 13478.
[39] S. P. O. Danielsen, G. E. Sanoja, S. R. Mccuskey, B. Hammouda, G. C. Bazan, G. H. Fredrickson, R. A. Segalman, *Chem. Mater.* **2018**, *30*, 1417.
[40] J. H. Ortony, R. Q. Yang, J. Z. Brzezinski, L. Edman, T.-Q. Nguyen, G. C. Bazan, *Adv. Mater.* **2008**, *20*, 298.
[41] S. P. O. Danielsen, B. J. Thompson, G. H. Fredrickson, T.-Q. Nguyen, G. C. Bazan, R. A. Segalman, *Macromolecules* **2022**, *55*, 3437.
[42] S. P. O. Danielsen, E. C. Davidson, G. H. Fredrickson, R. A. Segalman, *ACS Macro Lett.* **2019**, *8*, 1147.
[43] Y. Li, H. Shao, Z. Lin, J. Lu, L. Liu, B. Duployer, P. O. Å. Persson, P. Eklund, L. Hultman, M. Li, K. Chen, X.-H. Zha, S. Du, P. Rozier, Z. Chai, E. Raymundo-Piñero, P.-L. Taberna, P. Simon, Q. Huang, *Nat. Mater.* **2020**, *19*, 894.
[44] K. Tybrandt, I. V. Zozoulenko, M. Berggren, S. Adv, **2017**, *3*, eaao3659.
[45] F. Barbir, in *PEM Fuel Cells*, 2nd Ed. (Ed: F. Barbir), Academic Press, Boston, **2013**, pp. 33–72.
[46] J. Bobacka, A. Lewenstam, A. Ivaska, *J. Electroanal. Chem.* **2000**, *489*, 17.
[47] M. Bianchi, S. Carli, M. Di Lauro, M. Prato, M. Murgia, L. Fadiga, F. Biscarini, *J. Mater. Chem.* **2020**, *8*, 11252.
[48] D. A. Koutsouras, P. Gkoupidenis, C. Stolz, V. Subramanian, G. G. Malliaras, D. C. Martin, *ChemElectroChem* **2017**, *4*, 2321.
[49] S. Ghosh, O. Inganäs, *Adv. Mater.* **1999**, *11*, 1214.
[50] J. A. Rard, D. G. Miller, *J. Chem. Eng. Data* **1980**, *25*, 211.
[51] E. Stavrinidou, P. Leleux, H. Rajaona, D. Khodagholy, J. Rivnay, M. Lindau, S. Sanaur, G. G. Malliaras, *Adv. Mater.* **2013**, *25*, 4488.